Accepted version of manuscript. DOI 10.1007/s11370-018-0267-8
(The printed version of manuscript can be found at [https://doi.org/10.1007/s11370-018-0267-8])

Design of a 3D-printable, robust anthropomorphic robot hand including intermetacarpal joints

Won Suk You[1] · **Young Hun Lee**[2] · **Hyun Seok Oh**[2] · **Gitae Kang**[2] · **Hyouk Ryeol Choi**[2,*]

Received: 15 May 2018 / Accepted: 16 October 2018

Abstract This paper presents a new mechanical design of an anthropomorphic robot hand. The hand is designed such that it is adaptive, backdrivable, modularized to provide both dexterity and robustness. The hand has 18 joints, 14 degrees of freedom, and a new joint mechanism called an active DIP–PIP joint for the robot finger. The mechanism includes a pair of movable pulleys and springs for generating both linked and adjustable motions. Although the set of DIP(distal interphalangeal) and PIP(proximal interphalangeal) joints exhibits a coupled movement in free space, it moves adaptively when it contacts an object. To ensure a 1:1 ratio movement when a finger is moving freely and to produce additional joint torque when gripping an object, torsion springs are attached to each joint. The backdrivability of each joint is realized using an actuation module with a miniature BLDC motor and a ball screw. In addition, the relatively unknown intermetacarpal joints, which provide additional dexterity to the hand for grasping small objects, are used in the robot hand model. A modularized design simplifies the assembly of the hand and increases the economic feasibility. Experimental results are included in this paper for validating the design of the robot hand.

Keywords Multifingered hands, Mechanism design, Kinematics, Tendon driven, Backdrivable joint

Won Suk You[1]
Mechanical, Industrial, and Manufacturing Engineering, Oregon State University, Corvallis, USA
E-mail: youw@oregonstate.edu

Hyouk Ryeol Choi[2,*]
School of Mechanical Engineering, Sungkyunkwan University, Jangan-gu, Suwon, Kyungki-do, 440-746, Korea
Tel.: +82-031-290-7928
E-mail: hrchoi@me.skku.ac.kr

1 Introduction

The existing robot hands have been designed with several actuators to drive each joint of the hand [1]-[5]. In particular, the DLR hand [6] has 19 degrees of freedom (DOFs), and each joint of the DLR hand is actuated antagonistically by using two motors; thus, 38 motors are used. Recently, underactuated low-cost robot grippers have been developed using the three-dimensional (3D) printing technology [7]-[10]. These robot hands are mostly composed of soft materials and unique mechanisms capable of grasping objects adaptively without complicated control algorithms. In addition, using a 3D printer and less number of motors for driving a robot hand reduces the manufacturing time and cost. Ma *et al.* [11] developed a modular 3D-printed underactuated hand. The hand is designed with a hybrid pulley/whiffletree differential mechanism and flexure joints, which are made of low-cost materials and 3D-printed parts (less than USD 500). Kontoudis *et al.* [12] proposed an anthropomorphic, underactuated robot hand with a selectively lockable differential mechanism. The robot hand is actuated using a single motor, but several different postures are possible because of the lockable differential mechanism. Catalano *et al* [13] and Xu *et al.* [14] also proposed anthropomorphic underactuated robot hands. A continuum differential mechanism that uses elastic bars to increase the gripping force is proposed, and a novel robot hand called Pisa/IIT soft hand is designed based on adaptive synergies. Mitsui *et al* [15] proposed an underactuated robot hand that can grasp an object adaptively using elastic and idle pulleys. However, in the recently developed robot hands, each joint cannot be controlled independently because several DOFs are actuated using only a single motor.

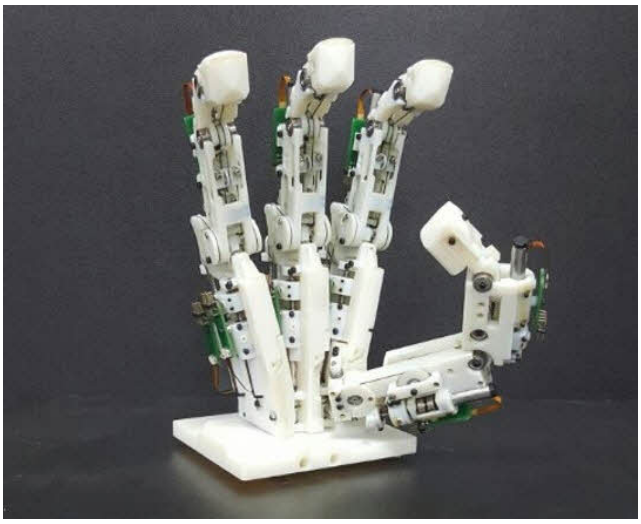

Fig. 1: Novel anthropomorphic robot hand, SKKU Hand V

For this reason, these grippers have limitations with respect to general manipulation tasks.

In this paper, we propose a 3D-printable anthropomorphic robot hand (Fig. 1), which has new joint mechanisms called active distal–proximal interphalangeal (ADP) joint and intermetacarpal (IMC) joints. An ADP joint is designed using a pair of movable pulleys. This mechanism allows the robot hand to rotate distal interphalangeal (DIP)/proximal interphalangeal (PIP) joint with a ratio of 1:1 in free space and grasp an object adaptively when it contacts the object. IMC joints are also used in the robot hand for enhancing the dexterity of in-hand manipulation. IMC joints are the joints formed in the palm between basis of the adjacent fingers. In addition, all the joints of the developed robot hand are backdrivable because of a mechanism composed with miniature BLDC motor and a ball screw. The backdrivable mechanism provides a natural protection against unexpected external impacts and enables the measurement of the tendon force via motor current. In this study, the robot hand shown in Fig. 1 is manufactured and its feasibility is demonstrated.

This paper is organized as follows: Firstly, the kinematic design of the robot hand is explained in Sect. 2. The mechanical design including the IMC joints is introduced in Sect. 3. In Sect. 4, the experimental evaluation of the proposed robot hand is discussed for verifying the performance of the hand. Lastly, our conclusions are presented in Sect. 5.

2 Kinematic design of the robot hand

The SKKU Hand V is developed based on the previous study on kinematic design optimization of an anthropomorphic robot hand [16]. It includes construction of mathematical model of robot hand and advantage of application of intermetacarpal (IMC) joints which are explained briefly in this section.

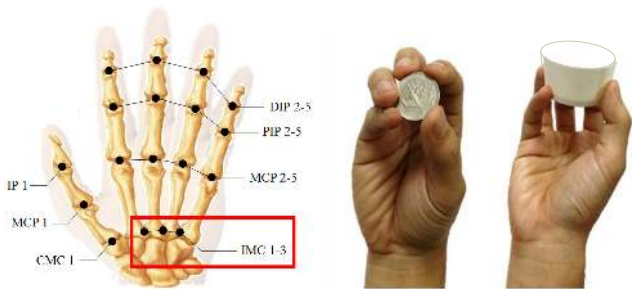

(a) Human hand's joints [18] (b) Cupping motion

Fig. 2: Illustration of the **a** joints and **b** cupping motion of human hand [16]

2.1 Mathematical model of robot hand

The human hand is capable of moving with 22 DOFs and weighs approximately 400 g. The fingers of the human hand can be categorized into two groups : the thumb and the remaining four fingers. The thumb is composed of the distal phalange (DP), proximal phalange (PP), and metacarpal phalange. All the phalanges and bones are connected to the interphalangeal (IP) joint, metacarpophalangeal (MCP) joint, and carpometacarpal (CMC) joint also known as saddle joint. Unlike the thumb, the other four fingers are composed of the DP, medial phalange (MP), PP, and metacarpal bone. The DIP joint, PIP joint, and MCP joint connect each phalange of an index, middle, ring, and little finger. As shown in Fig. 2, three joints are involved in the movement of each finger: the MCP, PIP, and DIP joints. The ranges of motion (ROMs) of these three joints account for the functional movement of each finger [17].

From the index finger to the little finger, the PIP and DIP joints show flexion–extension motion and the MCP joint exhibits both flexion–extension (FE) and abduction–adduction (AA) motion. To eliminate the redundancy of these fingers, the mobility of the fingers with four DOFs is redesigned with three DOFs similar to the human finger. In the field of biomechanics, the thumb is described as having five DOFs [22]-[25]; however, the thumb with four DOFs is adequate for a robot hand to carry out complex manipulation tasks as shown by the manipulation ability of several state-of-the-art robot hands [3][4][6]. Therefore, the fingers and the thumb of the hand model have three DOFs and four DOFs, respectively.

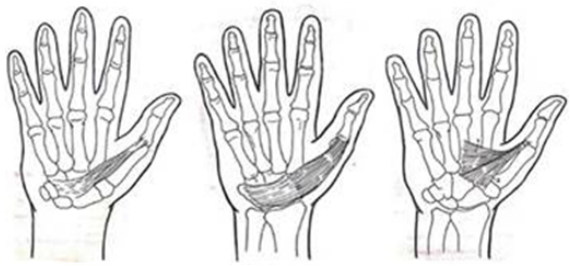

Fig. 3: Depiction of pollicis muscle [20].

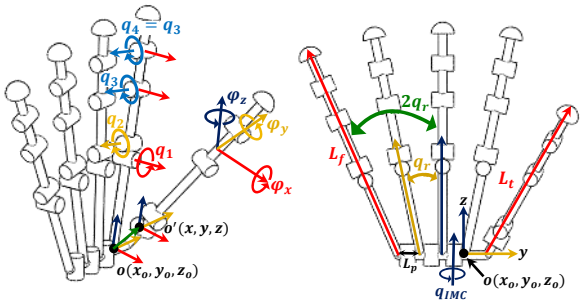

Fig. 4: Illustration of the hand model and its variables

In addition, the IMC joints exist in the palm of the human hand. These relatively unknown joints are formed between the metacarpal bones of the index, middle, ring, and little fingers' as shown in the red box of Fig. 2a. The IMC joints allow the human hand to perform a cupping motion as shown in Fig. 2b. Particularly, the cupping motion is proven to be at least 75% advantageous for performing pinch grip on small objects [16]; however, no robot hand has been designed to include the IMC joints in its palm. Moreover, because of the pollicis muscle (Fig. 3), the IMC and CMC joints of the human hand also exhibit coupled movement. This characteristic can be used in the control strategy of the robot hand so that the use of IMC joints does not increase the complexity of control.

To design the kinematic structure of a robot hand, the ROM should be defined. Several researchers have reported human hand's ROM of each joint [18][19]. The highest ROM in the PIP joint is approximately 123°, whereas the DIP joint exhibits a ROM of 101°-107°. In the MCP joint, the range of FE increases from 93° (thumb) up to 153° (little finger), whereas the ROM of the AA movement varies between 35° and 51°, and the IMC joints move approximately 20°. To calculate the inverse kinematics easily, the ROM of each joint is defined in a simple manner as shown in Table 1. The IMC joint rotates 20° whereas the CMC joint flexes 90°.

Table 1: Range of motion of each joint (°)

	Thumb [FE(AA)]	Fingers [FE(AA)]
CMC $[\theta_{t2}(\theta_{t1})/-]$	70(±30)	-
MCP $[\theta_{t3}/\theta_2(\theta_1)]$	90(-)	90(±20)
PIP $[-/\theta_3]$	-(-)	90(-)
DIP $[\theta_{t4}/\theta_4]$	90(-)	90(-)

FE flexion–extension, *AA* abduction–adduction

Table 2: Optimized mathematical model of robot hand (mm, °)

	Length of thumb	Length of fingers (index to little)
Metacarpal (L_{t1}/L_1)	73.5	92.5
Proximal phalanx (L_{t2}/L_2)	51.0	57.0
Middle phalanx (L_{t3}/L_3)	43.0	30.5
Distal phalanx $(-/L_4)$	-	25.5
L_p/q_r	20	12
$[x\ y\ z]/[\varphi_x\ \varphi_y\ \varphi_z]$	[11 -2 0]	[-39 -42 -40]

The length of the fingers varies widely between men and women and between children and adults. However, all of them perform manipulation tasks well because the lengths of the metacarpal bone, PP, MP, and DP compose a Fibonacci sequence, which makes the tip of a finger to draw an equiangular spiral during flexion. It allows the human hand to grasp objects with both the fingers and the palm [21]. Including this feature, the lengths of the fingers (L_f, L_t), angle between neighboring metacarpals (q_r), distance between neighboring junctions of metacarpal and carpal (L_p), and the orientation of the CMC joint ($[x\ y\ z]$, $[\varphi_x\ \varphi_y\ \varphi_z]$) of the robot hand are determined via optimization method to get the highest pinch grip capability in previous work [16], as shown in Fig. 4 and Table 2. The model of robot hand is prone to breakages because of the weak solidity of the material of the 3D-printed frame. Hence, the model is made 1.5 times bigger than the human hand to prevent it from breaking.

3 Mechanical design of the robot hand

In this section, the mechanical design of a novel 3D-printable anthropomorphic robot hand, which has new joint mechanisms called ADP and IMC joints, is presented. The ADP joint is designed using a pair of movable pulleys. This mechanism allows a robot hand to rotate the DIP/PIP joint with a ratio of 1:1 in free space and to grasp adaptively when it contacts an object. The IMC joints introduced in Sect. 2 are also used in the robot hand for enhancing the dexterity of in-hand

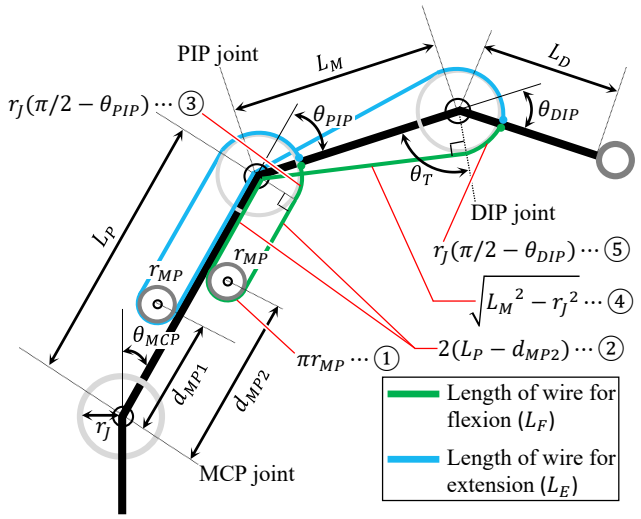

Fig. 5: Schematic diagram of robot finger with ADP joint

manipulation. In addition, all the joints in the developed robot hand are backdrivable because of a mechanism composed of a miniature BLDC motor and a ball screw. Backdrivable mechanisms provide a natural protection against unexpected external impacts and enable the measurement of the tendon force using the motor current.

3.1 Development of the robot finger module

3.1.1 Mathematical model of ADP joint

Firstly, a mathematical model of the ADP joint is constructed as shown in Fig. 5 and Eqs. 1–5. The joint is composed of a pair of movable pulleys that are located inside the proximal phalanx of the finger. The radius of the movable pulley (r_{MP}) is defined as half the radius of the joint pulley (r_{J}) for the convenience of calculation, and the movable pulleys are connected to each other with a tendon. L_{P}, L_{M} and L_{D} denote the length of the PP, MP, and DP, respectively. The original position of both the movable pulleys ($d_{\mathrm{MP1,O}}$, $d_{\mathrm{MP2,O}}$) is set as $L_{\mathrm{P}}/2$. Thus, the angle related to r_{J}, L_{M}, and θ_{T} can be written as follows:

$$\theta_{\mathrm{T}} = \cos^{-1}(r_{\mathrm{J}}/L_{\mathrm{M}}) \tag{1}$$

The lengths of the wires for flexion (L_{F}) and extension (L_{E}) can be expressed using Eqs. 2 and 3 (Fig. 5), respectively, based on the original position ($d_{\mathrm{MP1,O}}$, $d_{\mathrm{MP2,O}}$) of each movable pulley when the DIP and PIP joints are not rotated ($\theta_{\mathrm{DIP}} = 0,\ \theta_{\mathrm{PIP}} = 0$). The calculated values of L_{F} and L_{E} are constant.

$$\begin{aligned} L_F =& ① + ② \times 2 + ③ + ④ + ⑤ \\ =& 2(L_{\mathrm{P}} - d_{\mathrm{MP2,O}}) + \pi(r_{\mathrm{MP}} + r_{\mathrm{J}}/2) \\ &+ r_{\mathrm{J}}(\pi - \theta_{\mathrm{T}}) + \sqrt{L_{\mathrm{M}}^2 - r_{\mathrm{J}}^2} \end{aligned} \tag{2}$$

$$\begin{aligned} L_E =& 2(L_{\mathrm{P}} - d_{\mathrm{MP1,O}}) + \pi(r_{\mathrm{MP}} + r_{\mathrm{J}}/2) \\ &+ r_{\mathrm{J}}(\pi - \theta_{\mathrm{T}}) + \sqrt{L_{\mathrm{M}}^2 - r_{\mathrm{J}}^2} \end{aligned} \tag{3}$$

By using the lengths of the wires for flexion L_F/extension L_E, which are calculated from Eq. 2 and 3, and the angles of the DIP (θ_{DIP})/PIP (θ_{DIP}) joints, we can express the position of each movable pulley required to rotate the finger joints as follows:

$$\begin{aligned} d_{\mathrm{MP1}} =& L_{\mathrm{P}} + \Big(\pi r_{\mathrm{MP}} + \sqrt{L_{\mathrm{M}}^2 - r_{\mathrm{J}}^2} - r_{\mathrm{J}}\Big(\theta_{\mathrm{PIP}} + \theta_{\mathrm{DIP}} \\ &+ \theta_{\mathrm{T}} - 3\pi/2\Big) - L_{\mathrm{E}}\Big)/2 \end{aligned} \tag{4}$$

$$\begin{aligned} d_{\mathrm{MP2}} =& L_{\mathrm{P}} + \Big(\pi r_{\mathrm{MP}} + \sqrt{L_{\mathrm{M}}^2 - r_{\mathrm{J}}^2} + r_{\mathrm{J}}\Big(\theta_{\mathrm{PIP}} + \theta_{\mathrm{DIP}} \\ &- \theta_{\mathrm{T}} + 3\pi/2\Big) - L_{\mathrm{F}}\Big)/2 \end{aligned} \tag{5}$$

The expected motion of a robot finger with the ADP joint is presented in Fig. 6. Blue and green wires are contacted with movable pulleys 1 and 2, respectively. A yellow wire connects the two movable pulleys. The red zone represents the path that movable pulleys can take. For flexion movement, movable pulley 2 pulls down each wire attached to the PIP and DIP joints simultaneously. Similarly, when movable pulley 1 pulls down both the wires simultaneously, the robot finger is extended. Therefore, the DIP and PIP joints are rotated with a ratio of 1:1 in free space. The DIP and PIP joints of a robot finger are rotated with a ratio of 1:1 before the finger contacts an object. If the middle phalanx of the robot finger encounters an object during flexion, the object obstructs the PIP joint. Nevertheless, the DIP joint can flex to hold the object independently because the movable pulley 1 can pull down a wire attached only to the DIP joint. As a result, a robot finger with an ADP joint can grip an object firmly by using all the phalanges.

3.1.2 Design of ADP joint module

The most challenging part in the design of the robot finger was the realization of the movable pulleys and their paths in the proximal phalanx. Various attempts have been made to design a movable pulley and its path. The design of a movable pulley and its path is focused on reducing both the complexity of mechanism and the

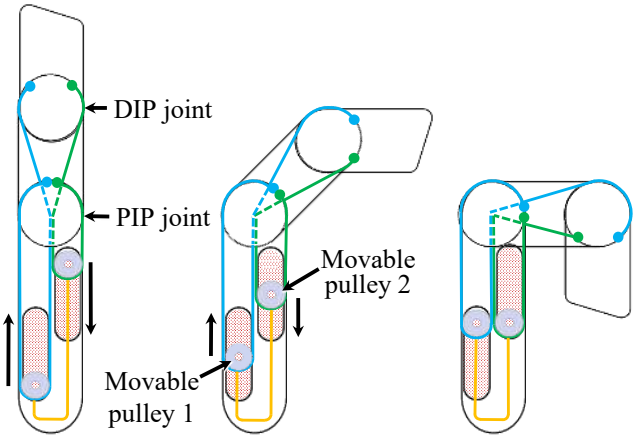

(a) Movement of ADP joint in free space

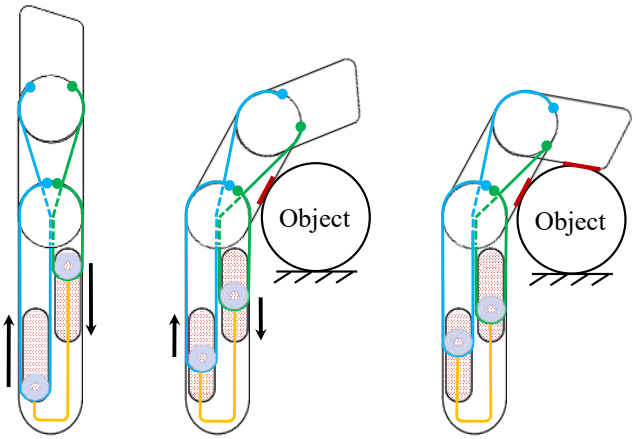

(b) Movement of ADP joint when blocked by object

Fig. 6: Expected movement of the ADP joint **a** in free space and **b** when middle phalanx is blocked by an object

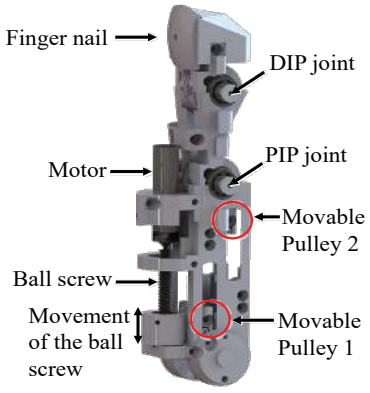

(a)

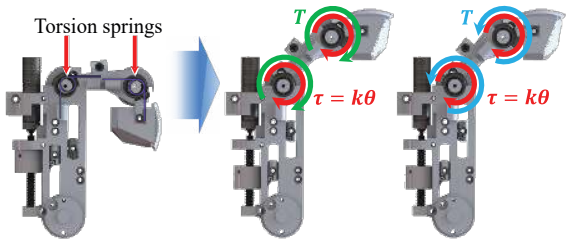

(b)

Fig. 7: Novel design of robot finger with ADP joint **a** configuration of designed robot finger and **b** application of torsion springs at each joint as fully flexed state (neutral posture) and torque when robot finger is flexed and extended

friction between the movable pulley and the tendon. In this design, the movable pulleys do not contact the frame of the proximal phalanx. In other words, there is no friction between a movable pulley and its path. To realize this design, the movable pulleys should not be tilted while moving through the path. Therefore, both the movable pulleys are connected to each other with two tendons, and each movable pulley pulls one tendon that is attached to the joint pulleys of the DIP and PIP joints.

The design of the MP/DP including the DIP/PIP joint is straightforward. Both the MP and DP are designed as two parts. One is the left half of the frame of the phalanx that is merged with joint pulley, and the other is the right half of the phalanx. A fingernail is also used to provide the robot hand with the capability of picking up thin objects, such as credit cards, lying on the floor. A linear movement of the movable pulley is realized using an actuation system, which consists of a ball screw and a motor (Fig. 7a). The actuated movable pulley is driven by this actuation system and the other movable pulley is steered by the tendons that link the movable pulleys with each other. In addition, torsion springs are connected to the DIP and PIP joints of the robot hand as shown in Fig. 7b. The initial posture of a typical robot hand is defined as the fully extended state. However, in case of the developed robot finger, the initial posture is defined as the fully flexed state. The torsion spring generates additional joint torque with its elastic force when the robot hand grasps an object. The actuator has to generate more force than that required for extending the finger because of the elastic force of the torsion spring; however, the actual work will be done by the robot hand when it grips or grasps various objects. In other words, sacrificing maximum extension torque and getting additional torque using the elastic component when flexing the finger is a reasonable trade-off.

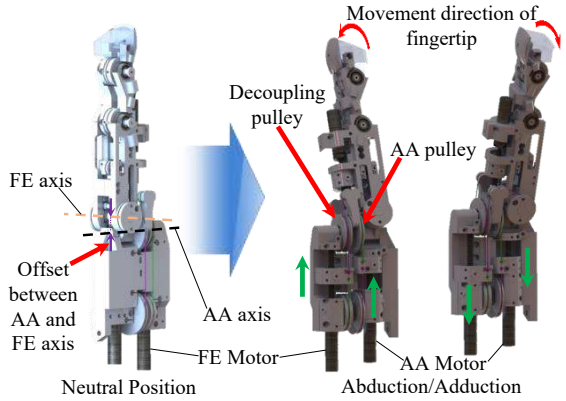

(a) Abduction and adduction movement of MCP joint.

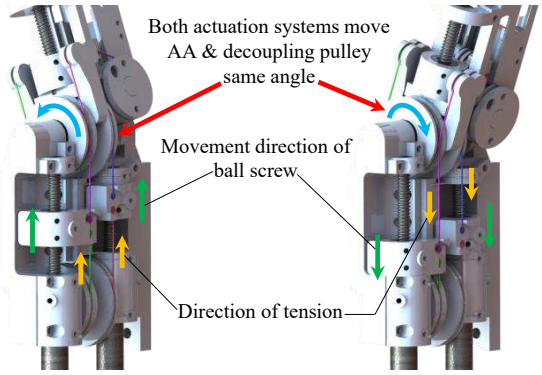

(b) Operation principle of the decoupling pulley for AA.

Fig. 8: Abduction and adduction **a** movement of MCP joint, and **b** operation principle of the decoupling pulley for AA.

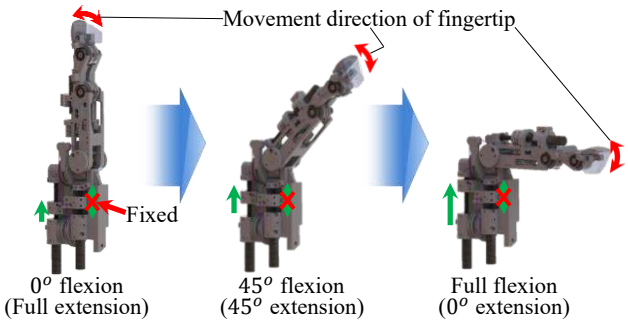

(a) Flexion and extension movement of MCP joint

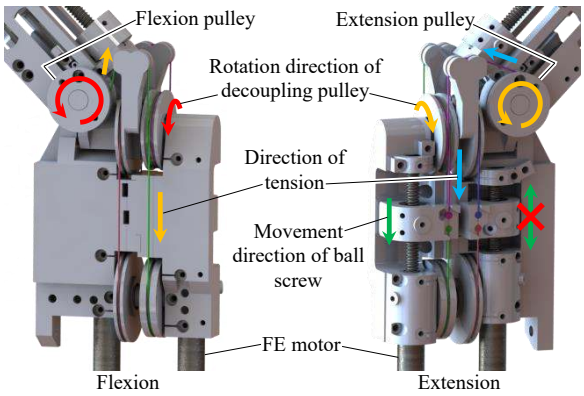

(b) Operation principle of the decoupling pulley for FE

Fig. 9: Flexion and extension **a** movement of MCP joint, and **b** operation principle of the decoupling pulley for FE.

3.1.3 Design of MCP joint module of robot finger

Because the MCP joint has two DOFs–AA and FE, the decoupling of these two DOFs should be carefully considered at the design level to reduce the complexity of control. As shown in Fig. 8a, the developed MCP joint module has two sets of actuation systems consisting of a ball screw and a motor. The AA motor generates a linear motion with the ball screw. Then, the tendon-attaching part, which is used for linking the nut of the ball screw and the tendon, causes AA movement by pulling the red or blue tendon with the directions of orange arrows shown in Fig. 8b.

For easy decoupling, a decoupling pulley that can be independently rotated without affecting AA pulley is included behind the AA pulley. As shown in Fig. 9, both the flexion (green) and extension (purple) tendons of the MCP joint are wound on the decoupling pulley before attaching to the FE pulley (Fig. 9a). For the abduction or adduction of the MCP joint without any flexion or extension, we need to rotate both the AA pulley and the decoupling pulley with the same angle with the directions of blue arrows (Fig. 8b) using the AA and FE motors of the MCP joint. Although the AA system can abduct the MCP joint when the FE motor is fixed at any position, it will exhibit an unwanted diagonal movement.

On the other hand, for the flexion or extension of the MCP joint without any abduction or adduction movement (Fig. 9a), we need to actuate the FE motor to pull green (flexion) or purple (extension) tendon with the directions of orange or blue arrows, respectively, as shown in Fig. 9b, while the AA motor holds its current position. The decoupling pulley allows the robot finger to generate MCP joint's FE movement without AA movement. Although the axes of the MCP joint of the human hand are orthogonal, the MCP joint of the finger module is designed to have an offset between the AA and FE axes. As the two movable pulleys and a guidance pulley of the tendon, which connects the movable pulleys with each other, are located in the proximal phalanx module, it was hard to make the AA and FE axes orthogonal without any conflict between nearby frames.

3.2 Design of intermetacarpal (IMC) joints

The IMC joints are the joints existing between the adjacent metacarpal bones that allow the human hand to gather all the five fingers at one point. This enlarges the possible area for precision gripping (for two- and three-finger pinch). As proved using the workspace intersection volumes in Sect. 2, the IMC joints are worth including in the robot hand. The human IMC joints exhibit coupled movement, so the designed IMC joints are also coupled with each other as shown in Fig. 10. Joint IMC1 is connected to the tendon-driving system using a ball screw. When the tendon-driving system pulls tendon T1, IMC1 rotates by θ_{IMC1}. Because tendons T2 and T3 are fixed to frame 1 and frame 3, respectively, the rotation of IMC1 winds tendon T2 wrapping around IMC1 and pulls tendon T2 on IMC2. Similarly, the rotation of IMC1 unwinds tendon T3 on IMC1 and winds tendon T3 wrapping around IMC2. The same mechanism is applied to joint IMC3. Therefore, the rotation angle of IMC2 (θ_{IMC2}) and that of IMC3 (θ_{IMC3}) are the same as the rotation angle of IMC1 (θ_{IMC1}).

The designed IMC joint module and its actuation system are illustrated in Fig. 11. At the bottom of the IMC joint module, bearings are implanted as wheels for supporting the weight of the module and for the smooth movement of the IMC joints. The actuation system is located on the lateral side of the index finger frame of the IMC joint. In addition, the motion of the IMC joint is coupled with the FE of the CMC joint similar to that of the human hand in which it is also coupled to the pollicis muscle [20]. Therefore, it is possible to use the IMC joints in the robot hand without increasing the complexity of control.

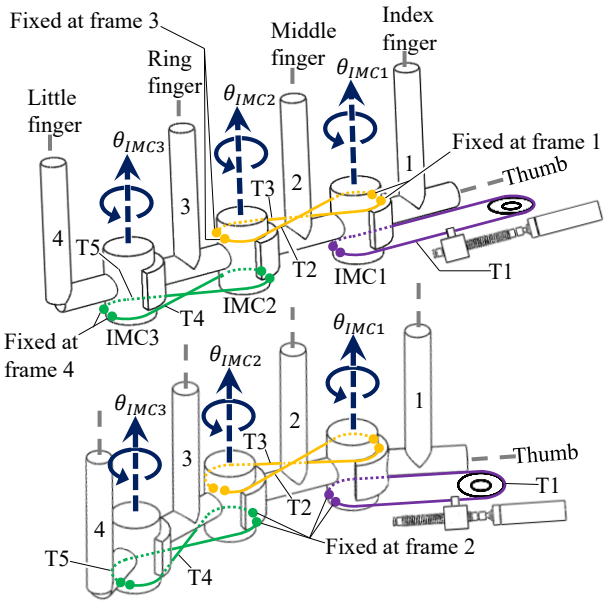

Fig. 10: Schematic depiction of IMC joint mechanism

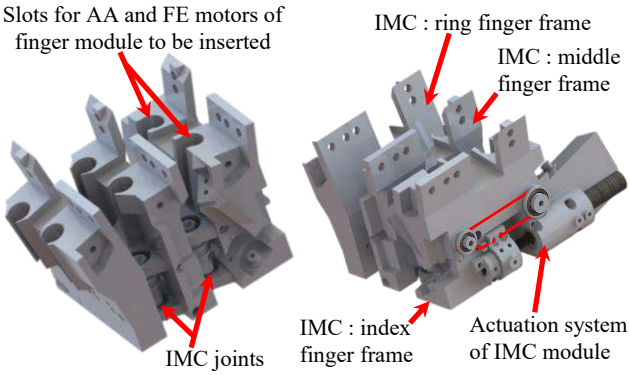

Fig. 11: Design of IMC joint module and its actuation system

3.3 Design of thumb module

The thumb module of the robot hand consists of four joints : the CMC FE joint, CMC AA joint, MCP joint, and interphalangeal (IP) joint as shown in Fig. 12. Among those joints, the actuation systems of three joints are integrated to the thumb, whereas the actuation system of the CMC AA joint is located on the medial-lateral side of the IMC : index finger frame, which is on the opposite side of the location of the actuation system of the IMC joints. The actual assembling sequence of the IMC and the thumb modules is such that the assembled thumb is integrated first with the IMC : index finger frame and then followed by the remaining parts of the IMC joint module. Considering the fact that the CMC FE pulley of most of the robot hands is on the metacarpal, which is driven by an actuation system located in the palm, the characteristics such as having the actuation system of the FE joint mounted on the metacarpal of the thumb and driving the FE joint by pulling a tendon fixed on the CMC FE pulley are quite unique.

3.4 Design of actuation system

3.4.1 A backdrivable mechanism

The robot hand has total 18 joints actuated using 14 motors, four fingers including the thumb, and two IMC joints located in the palm as shown in Fig. 13. An actuation system is designed with a backdrivable mech-

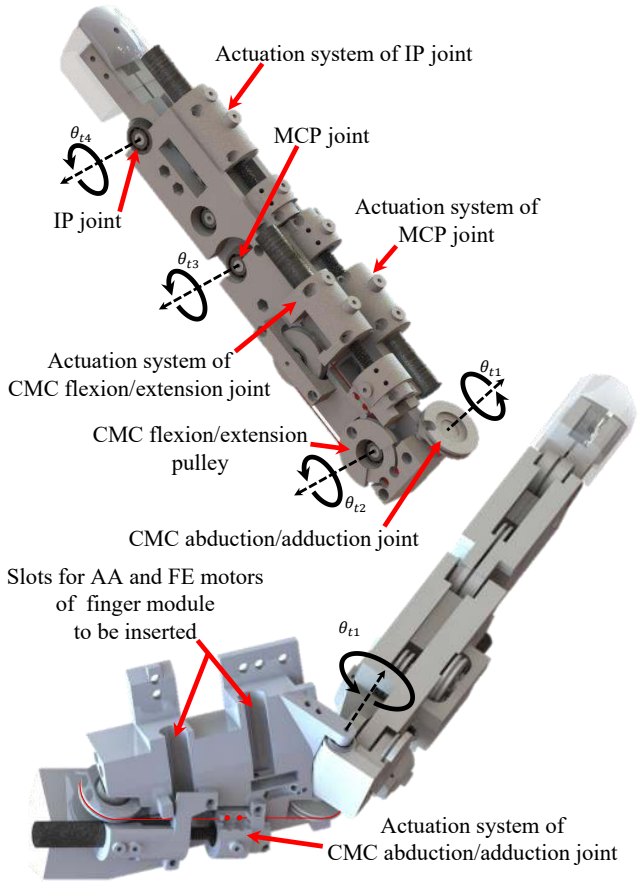

Fig. 12: Design of thumb module

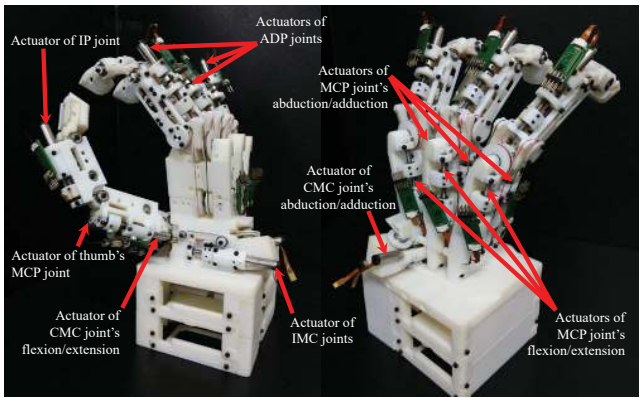

Fig. 13: Illustration of the developed robot hand and locations of actuators.

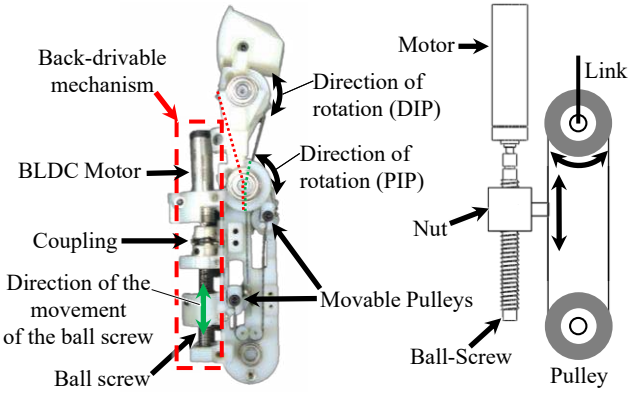

Fig. 14: Actuation system including backdrivable mechanism in the ADP joint and schematic of the backdrivable mechanism.

anism to develop a robot hand using a lesser number of motors than its DOFs, such as the IMC joints and each of the ADP joints that require only one motor to be driven.

All the joints are actuated using backdrivable mechanisms consisting of a miniature BLDC motor and a ball screw. The mechanism is adopted from previous research works [3][26] with some modifications. In this study, the backdrivable mechanism comprises a miniature BLDC motor (Maxon EC8) and a ball screw (Eichenberger ZYI 4×1) as shown in Fig. 14. The actuation system (tendon-driving system) is designed with this backdrivable mechanism. As shown in Fig. 14, the rotation of the motor generates a linear motion of the nut of the ball screw, which bidirectionally pulls a tendon attached to the joint pulley. Thus, the joint can be actuated in both the directions using one motor. The first advantage of adopting a backdrivable mechanism in the robot hand is that a minimum number of tendons and pulleys are used because a single motor can actuate a one-DOF motion in each direction. Compared to the fact that, generally, two motors are required to drive a one-DOF joint in tendon-driven robot hands, this feature is a big merit for the tendon-driven robot hand.

In the design of the robot hand, three different lengths of ball screws and three types of motors with different gear ratios are used, as listed in Table 3. Using the knowledge of the ball screw, motor, gear head, and ROM, we theoretically calculated the resolution of each joint that the actuation system can control. Firstly, to derive the resolution of each joint the actual usage length (L_a) of each joint should be calculated using Eq. 6 where r_p and ROM are the relevant joint pulley radius (radian) and the ROM of each joint, respectively. Here, the relevant joint pulley radius means the sum of the joint pulley radius and half of the thickness of the tendon. Then, as shown in Table 4, the resolution (θ_res) of each joint is derived using Eq. 7 where p_b is the pitch of the ball screw, GR is the gear ratio of the gear head, and h_p is the number of poles of the hall sensors embedded in the motors.

Table 3: List of ball screw lengths and gear ratios of motors in actuation system of each joint

Name of the joint	Length of ball-screw (mm)	Gear ratio
ADP joint of finger	25	4:1
FE joint of finger's MCP joint	30	4:1
AA joint of finger's MCP joint	20	4:1
IP joint of thumb	20	4:1
MCP joint of thumb	20	4:1
FE joint of thumb's CMC joint	20	16:1
AA joint of thumb's CMC joint	20	16:1
IMC joint in palm	20	64:1

Table 4: Range of motion (ROM), relevant joint pulley radius (R), and theoretical resolution (Res.) of each joint that the actuation system can control.

Name of the joint	ROM (°)	R (mm)	Res. (°)
ADP joint of finger	90	7.51	0.64
FE joint of finger's MCP joint	90	8.65	0.55
AA joint of finger's MCP joint	40	12.75	0.37
IP joint of thumb	90	6.25	0.76
MCP joint of thumb	90	6.25	0.76
FE joint of thumb's CMC joint	70	8.75	0.14
AA joint of thumb's CMC joint	60	9.25	0.13
IMC joint in palm	20	4.2	0.071

$$L_{\mathrm{a}} = \frac{r_{\mathrm{p}}}{ROM} \tag{6}$$

$$\theta_{\mathrm{res}} = \frac{p_{\mathrm{b}} \cdot ROM}{L_{\mathrm{a}} \cdot GR \cdot h_{\mathrm{p}}} \tag{7}$$

Although the roughest resolution is 0.64°, the actual joint resolution is considered to be approximately 1° because of uncontrollable factors such as friction and misalignment of the assembly.

The backdrivable mechanism can measure the tendon force using the motor current. Many types of sensors such as force/torque sensors, which are used to obtain this information are very expensive. However, the backdrivable mechanism can measure the joint torque by using the characteristic of backdrivability, which is well matched with the recent trend that robot hands are being developed at a low cost. Practically, these

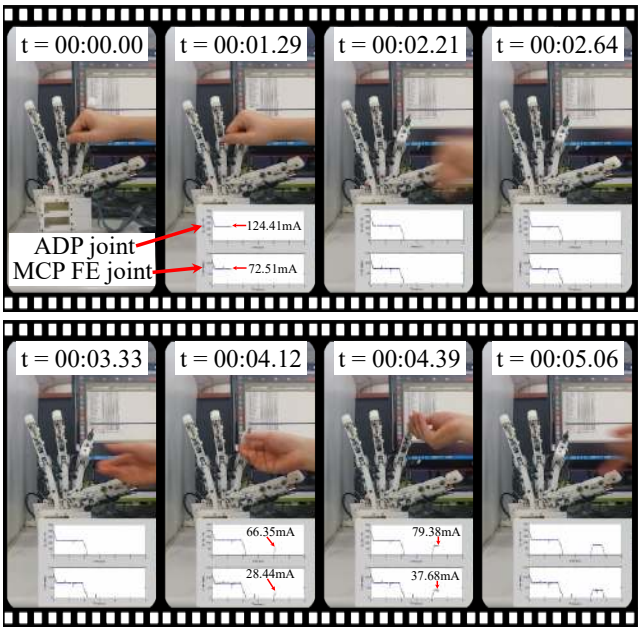

Fig. 15: Response of the robot hand when it faces unexpected obstacles with time stamp (Second).

mechanisms reduce the cost of the robot hand. Using the motor current and position-based stiffness control, the robot can sense an object when the tip of its finger contacts the object and can determine the joint torque exerted on the tendon. Moreover, backdrivable mechanism can provide a natural protection against unexpected external impacts. Therefore, even though the robot hand faces unexpected obstacles such as humans (Fig. 15) or the surrounding environment, both the robot and the obstacle can be protected from damage. This feature is especially helpful for 3D-printed robot hands, such as the proposed robot hand, which are more fragile than the traditional robot hands. Combining the backdrivable mechanism with stiffness control, the developed robot finger can even withstand the impact of a hammer as shown in Fig. 16.

To test the backdrivability of the joints, each joint of the fingers and the thumb module is indiscriminately rotated by hand. From this experiment, it is confirmed that all the joints can be actuated using the motor and rotated by external forces, without harming any structure or mechanism of the robot hand.

4 Gripping strategy for robot hand

To grip an object, the robot hand uses a general stiffness control method and the coordinate center of the workspace intersection volume, as shown in Fig. 17. The gripping strategy used in this study is the benchmark

Fig. 16: Impact experiment to show robustness of robot hand.

of the groped grasp [28]. The main difference is that the groped grasp uses a geometric centroid of the groped-shape, and the grip strategy for the developed robot hand uses the coordinate center of the workspace intersection volume.

When the robot hand grips an object, all the forces of the contact points should be directed toward the coordinate center of the workspace intersection volume (r_d), as shown in Fig. 18a. The direction of the contact force can be derived from the position relationship (Eq. 8) and the relation of magnitude, which can be calculated from the force equilibrium of Eq. 9,

$$\hat{\mathbf{f}}_i = \frac{\mathbf{r}_d - \mathbf{P}_i}{||\mathbf{r}_d - \mathbf{P}_i||} \tag{8}$$

$$\alpha_1\hat{\mathbf{f}}_1 + \alpha_2\hat{\mathbf{f}}_2 + \alpha_3\hat{\mathbf{f}}_3 = 0 \tag{9}$$

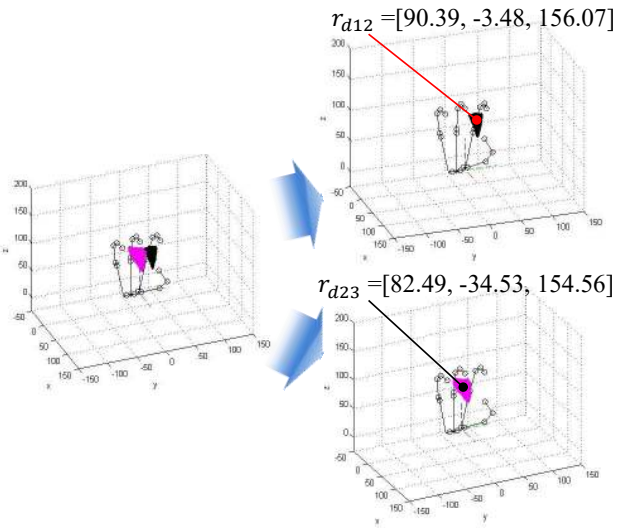

Fig. 17: Illustration of coordinate center of workspace intersection volume of three-finger pinch grip.

where α_i denotes the magnitude of contact force for maintaining the grip. Since Eq. 9 is nondeterministic, the magnitude (α_i) cannot be determined. However, the contact force can be regulated and actively redistributed among the contact positions for an active contact position.

To make it simpler, a linear relationship between the contact position and the coordinate center is applied, but any sophisticated distribution function or condition can be applied. The contact force dramatically changes the direction even if a small disturbance is imposed when the length between the contact position and the coordinate center is relatively large. Thus, a part of this problem can be avoided using the inversely proportional relationship as shown in Eqs. 10 and 11. The magnitude of the remaining force is determined from the equilibrium equation (Eq. 12).

$$||\mathbf{r}_d - \mathbf{P}_1|| : ||\mathbf{r}_d - \mathbf{P}_2|| = \alpha_2 : \alpha_1 \tag{10}$$

$$\alpha_2 = \frac{||\mathbf{r}_d - \mathbf{P}_1||}{||\mathbf{r}_d - \mathbf{P}_2||}\alpha_1 \tag{11}$$

$$\alpha_3 = ||\alpha_1\hat{\mathbf{f}}_1 + \alpha_2\hat{\mathbf{f}}_2|| \tag{12}$$

The magnitude of the force of the thumb (α_1) is the value that the user can assign freely. In other words, the value can be adjusted to give adequate force to maintain the grip or perform manipulation. The entire gripping force can be redistributed by changing α_1. The position

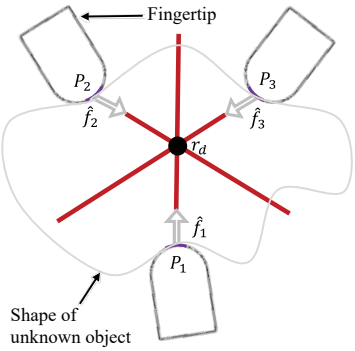

(a) Gripping strategy

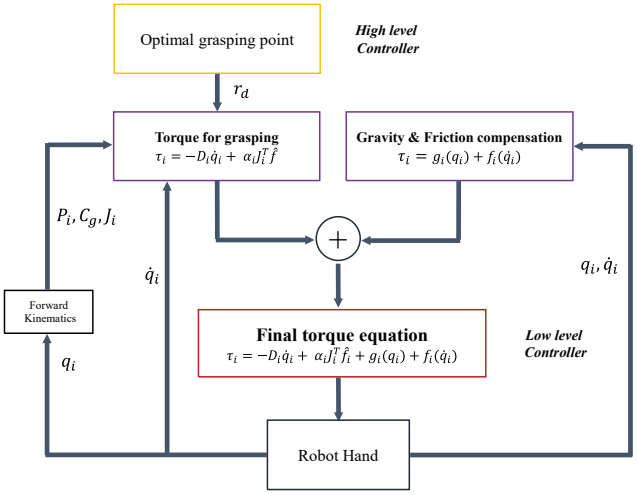

(b) Control scheme of the robot hand

Fig. 18: Depiction of **a** the gripping strategy and **b** the entire control scheme of the robot hand to grip an object.

of α_3 is defined as the pivot point and functions as a passive point. It does not give an active force, but only gives a force that can equilibrate the active forces. For the force equilibrium, any active point can be switched to the pivot point.

A control input for gripping can be given to the robot hand using Eq. 13, where D_i denotes a damping coefficient matrix, $\dot{q}_i$ is an angular velocity vector, and J_i is the Jacobian of each finger. The entire control scheme of the robot hand for gripping an object is shown in Fig. 18b.

$$\tau_i = -\mathbf{D}_i\dot{\mathbf{q}}_i + \alpha_i \mathbf{J}_i^T \hat{\mathbf{f}}_i \quad (i = 1, 2, 3) \tag{13}$$

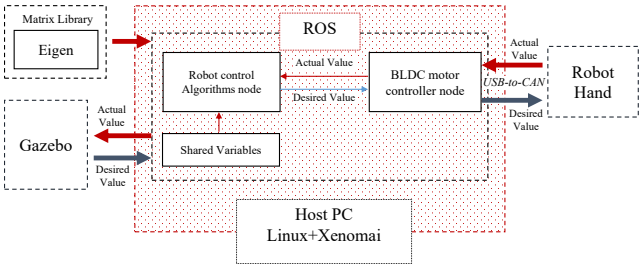

Fig. 19: Communication scheme for developed robot hand

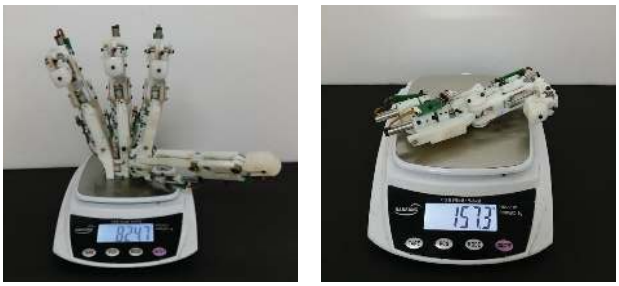

(a) (b)

Fig. 20: Weight of **a** robot hand and **b** single-finger module.

5 Experimental evaluation

The proposed robot hand has new joint mechanisms, called the active DIP–PIP (ADP) joint and the IMC joints. These mechanisms allow the robot hand to grasp an object easily and more naturally, without needing seriously complicated control algorithms. The ADP joint is intended to improve the ability of the power grip with its adaptive gripping a capability by developing new kind of differential joint mechanism. On the other hand, the IMC joint mechanism is adopted to enhance the precision grip capability by allowing the robot hand to do a cupping motion, so that the robot hand can gather three or more finger tips in a larger area than before. Therefore, an experimental evaluation of the robot hand's grasping capability is presented in this section.

5.1 Communication system

The communication system of the robot hand includes the Robot Operating System (ROS), Xenomai, and CAN protocol as illustrated in Fig. 19. Because the ROS is a collection of tools, libraries, and conventions that aim to simplify the task of creating complex and robust robot behavior, it serves as a middleware that offers good interfacing and helps with collaboration between

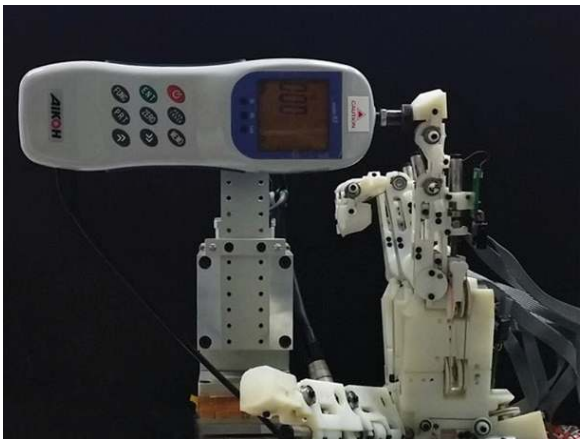

(a)

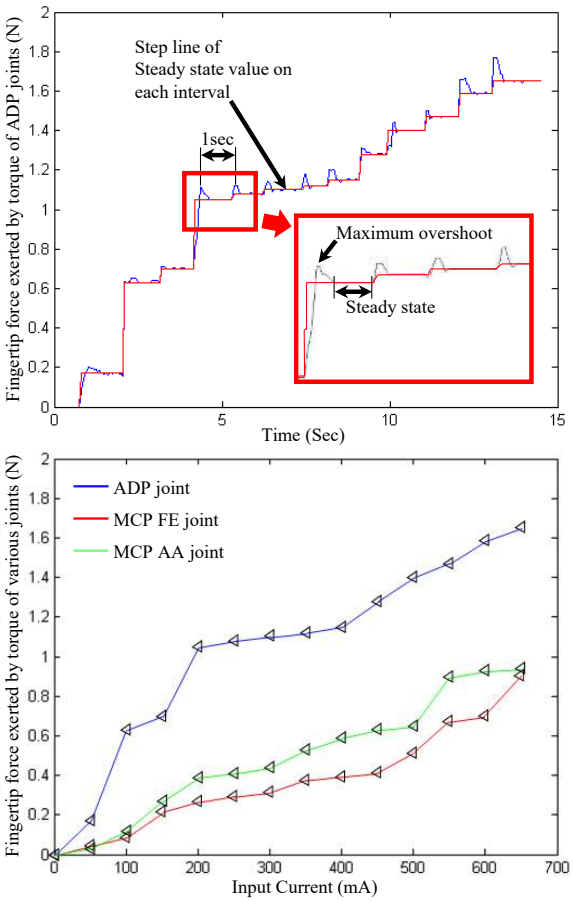

(b)

Fig. 21: Depiction of **a** the setup for testing fingertip force and **b** the results.

software. The communication system runs on the Linux platform, and the robot hand is operated in real time, particularly, with the help of Xenomai, which is a free, versatile software framework for implementing and migrating real-time applications based on standard APIs or accurate emulation of proprietary real-time operating system interfaces. In addition, the developed robot hand can be simulated using Gazebo. This simulation allows researchers to test their control algorithm without using an actual robot so that even if the algorithm shows unexpected behavior, the robot remains unharmed.

5.2 Weight and fingertip force of the robot hand

The total weight of the designed robot hand including the actuators is 824.7 g, and the weight of the single finger module is 157.3 g, as shown in Fig. 20. Although the robot hand is light in weight, it can still handle the objects that are frequently used in daily life. As shown in Fig. 21a, the experimental environment is set using a push–pull gage (0.01 N resolution) for testing the fingertip force of the finger module. Although the maximum input current is 690 mA, the test is carried out by inputting motor current from 50 mA to maximum 650 mA considering a safe margin with the increase of 50 mA every second. The maximum force of the fingertip that can be generated by the ADP joint, the FE joint of the MCP joint, and the AA joint of the MCP joint is 1.65 N, 0.91 N, and 0.94 N, respectively (Fig. 21b).

Calli et al. [27] used the objects that are frequently used in daily life to determine whether these maximum fingertip forces are adequate for gripping objects. The fingertip force required to perform pinch grip of an object can be calculated using Eq. 14 where m and g denote the mass of the object and the gravitational acceleration, respectively, μ is the coefficient of friction of the fingertip on the object, and n is the number of fingers used for pinch gripping.

$$F_{\text{tip}} = \frac{mg}{\mu n} \tag{14}$$

The average weight listed in the report is approximately 200 g. If the friction coefficient of the soft fingertip on the object is assumed as 0.5, which is the general coefficient of friction of rubber, the fingertip forces required to perform a two-finger pinch grip and a three-finger pinch grip are 1.96 N and 1.31 N, respectively. Since the designed robot hand can impose maximum fingertip forces of 1.65 N, 0.91 N and 0.94 N with the actuators of the ADP joint, the FE and AA joints of the MCP joint, respectively, the robot hand is able to perform both two-finger and three-finger pinches on an object of average weight.

5.3 Evaluation of gripping capability

The grip of the human hand can be classified into two categories : power gripping and precision gripping [29]. Thus, the performance of the designed robot hand is evaluated using both the grips by gripping daily-life objects. In the case of the power grip, simply rotating all the motors of the joints with a certain input current limit makes the robot hand grip an object stably because of the ADP joint. The ADP joint allows the robot hand to grip an object by contacting all its phalanges with the object. To verify this, the power grip is performed on various objects with radii ranging from 26 to 100 mm, as shown in Fig. 22a. On the other hand, the precision gripping capability is maximized in the design level by optimizing the structure of the robot hand. In other words, the structure of the robot hand itself is developed for precision gripping, particularly, for the two- and three-finger pinch grips. The precision gripping capability of the robot hand is evaluated by performing two-finger and three-finger pinch grips on everyday objects of radii ranging from 9 to 30 mm (Fig. 22b). Moreover, a lateral pinch grip is carried out on a 1-mm-thick card. With the movement of the IMC joint (Fig. 22b), even smaller objects such as coins of KRW 10 (9 mm radius) can be gripped with three as shown in Fig. 23. Although the grip control algorithm is not applied to either the power or the precision gripping experiment, the robot hand shows a good performance for both the grips.

After this preliminary evaluation, the aforementioned grip control algorithm is applied to the robot hand. As shown in Fig. 23, the index finger, middle finger, and thumb of the robot hand are directed to the coordinate center of the workspace intersection volume ($r_{d12} = [90.39, -3.48, 156.07]$). Then, the center of gravity of various objects, such as a rectangular sponge (25 mm thickness), a roll of insulation tape (30 mm radius), a paper cup (50 mm radius), and coins of KRW 100 (12 mm radius) and KRW 10 (9 mm radius) are located at this position. The results indicate that even tiny objects, such as coins of KRW 10, are easily gripped. Not many robotic hands have shown gripping capabilities for such small objects.

In summary, the above experimental evaluation shows good performance of the designed robot hand in performing both the power grip with an adaptive gripping capability of the ADP joint mechanism and the precision grip with the adoption of IMC joints in the palm. The robot hand shown in this study mainly aims on the precision grip. The other is the accessorial ability because the capability of precision gripping and that of adaptive gripping are on the edge of both sides.

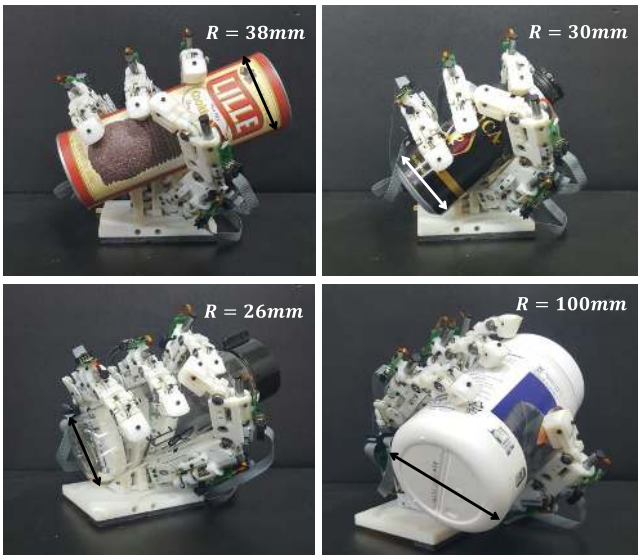

(a) Power grip experiment

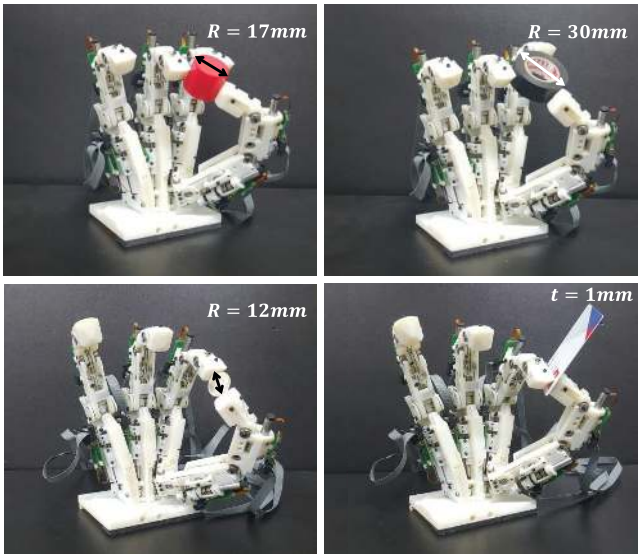

(b) Pinch grip experiment

Fig. 22: Illustration of **a** power grip experiment using advantages of ADP joint and **b** pinch grip experiment with three fingers and two fingers

6 Conclusion

In this paper, we proposed a new anthropomorphic robot hand including a backdrivable mechanism, an ADP joint, and IMC joints. The robot hand is developed to have closer dexterity the precision grip of the human hand without any complex control algorithm. In addition, the ADP joint mechanism is also an underactuated mechanism, but controlling both flexion and extension of DIP and PIP joints with a single motor is possible unlike other underactuated mechanisms, which control only

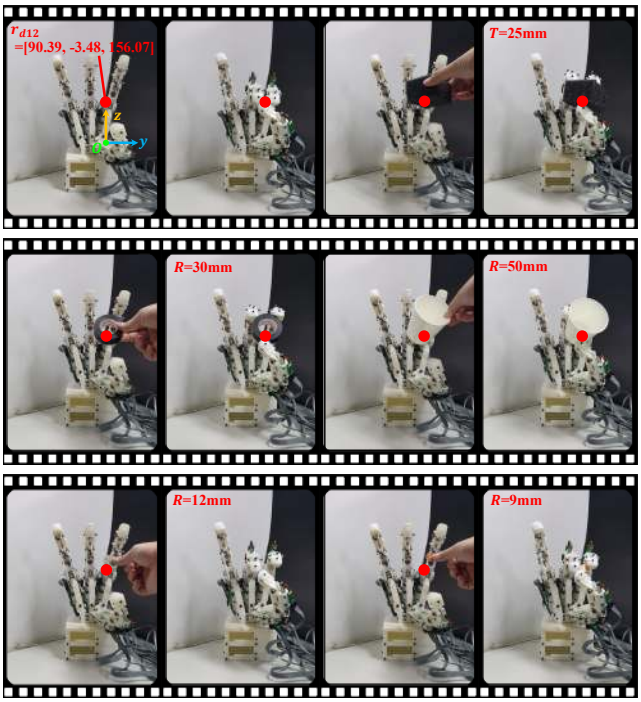

Fig. 23: Pinch grip capability evaluation using coordinate center of workspace intersection volume

the flexion and depend on elastic elements for extension. After assembling the robot hand, the power gripping and precision gripping of the developed robot hand are evaluated using our own gripping strategy in which the coordinate center of the workspace intersection volume of the robot fingers is used as the gripping point. This verified the high gripping capability of the developed robot hand.

In the future, the designed robot hand will be integrated with a robot arm for carrying out numerous gripping and manipulation tasks. The effectiveness of the proposed robot hand will be further evaluated in this process.

Acknowledgements This research was supported by the convergence technology development program for bionic arm through the National Research Foundation of Korea(NRF) funded by the Ministry of Science & ICT (No. 2014M3C1B20-48175).

References

1. Rothling F, Haschke R, Steil JJ, Ritter H (2007) Platform portable anthropomorphic grasping with the bielefeld 20-DOF shadow and 9-DOF TUM hand. In: International conference on intelligent robots and systems, San Diego, pp 2951–2956
2. Deshpande AD, Xu Z, VandeWeghe MJ, Brown BH, Ko J, Chang LY,Wilkinson DD, Bidic SM, Matsuoka Y (2011) Mechanisms of the anatomically correct testbed hand. IEEE/ASME Trans Mechatron 18:238–250
3. Bridgwater, LB, IhrkeCA, DiftlerMA, Abdallah ME,RadfordNA, Rogers JM,Yayathi S, AskewRS, LinnDM(2012) TheRobonaut 2 hand–designed to do work with tools. In: 2012 IEEE international conference on robotics and automation, Saint Paul, Minnesota, USA, pp 3425–3430
4. Melchiorri C, Palli G, Berselli G, Vassura G (2013) Development of the UB Hand IV: overview of design solutions and enabling technologies. IEEE Robot Autom Mag 20(3):72–81
5. Kim YJ, Kim J, Lee JW, Park KM, Roh KS, Choi JY (2014) RoboRay hand : a highly backdrivable robotic hand with sensorless contact force measurements. In: International conference on robotics and automation (ICRA), Hong Kong, pp 6712–6718
6. Grebenstein, M, Albu-Schäffer, A, Bahls T, Chalon M, Eiberger O, FriedlW, Gruber R,Haddadin S,HagnU,Haslinger R,HöppnerH, Jörg S, Nickl M, Nothhelfer A, Petit F, Reill J, Seitz N, Wimböck T, Wolf S, Wüsthoff T, Hirzinger G (2011) The DLR hand arm system. In: International conference on robotics and automation, Shanghai, China, pp 3175–3182
7. Odhner LU, Jentoft LP, Claffe MR, Corson N, Tenzer Y, Ma RR, Buehler M, Kohout R, Howe RD, Dollar AM (2014) A compliant, underactuated hand for robust manipulation. Int J Robot Res 33(5):736–752
8. Stuart HS, Wnag S, Gardineer B, Christensen DL, Aukes DM, Cutkosky M (2014) A compliant underactuated hand with suction flow for underwater mobile manipulation. In: International conference on robotics and automation (ICRA), Hong Kong, pp 6691–6697
9. Kuo P, DeBacker J, Deshpande AD (2015) Design of robotic fingers with human-like passive parallel compliance. In: International conference on robotics and automation (ICRA), Seattle, pp 2562–2567
10. Ma RR, Spiers A, Dollar AM (2016) M^2 Gripper: extending the dexterity of a simple, underactuated gripper. Adv Reconfig Mech Robots 36:95–805
11. Ma RR, Odhner LU, Dollar AM (2013) A modular, open-source 3D printed underactuated hand. In: International conference on robotics and automation (ICRA), Karlsruhe, pp 2722–2728
12. Kontoudis GP, Liarokapis MV, Zisimatos AG, Mavrogiannis CI, Kyriakopoulos KJ (2015) Open-source, anthropomorphic, underactuated robot hands with a selectively lockable differential mechanism: towards affordable prostheses. In: International conference on robotics and automation, Hamburg, pp 5857–5862
13. Catalano MG, Grioli G, Farnioli E, Serio A, Piazza C, Bicchi A (2014) Adaptive synergies for the design and control of the Pisa/IIT SoftHand. Int J Robot Res 33(5):768–782
14. Xu K, Liu H, Liu Z, Du Y, Zhu X (2015) A single-actuator prosthetic hand using a continuum differentialmechanism. In:Conference on robotics and automation (ICRA), Seattle, pp 6457–6462
15. Mitsui K, Ozawa R, Kou T (2013) An under-actuated robotic hand for multiple grasps. In: International conference on robots and system (IROS), Tokyo, pp 5475–5480
16. You WS, Lee YH, Kang G, Oh HS, Seo JK, Choi HR (2017) Kinematic design optimization of anthropomorphic robot hand using a new performance index. In: International conference on ubiquitous robots and ambient intelligence (URAI), Jeju, South Korea, pp 20–25

17. Yu H, Chase RA, Strauch B (2003) Atlas of hand anatomy and clinical implications. Mosby, Maryland Heights ISBN-13: 978-0815179276
18. Stillfried G, Smagt P (2010) Movement model of a human hand based onmagnetic resonance imaging (MRI). In: International conference on advances in bioscience and bioengineering
19. Cobos S, Ferre M, Uran MAS, Ortego J, Pena C (2008) Efficient human hand kinematics for manipulation tasks. In: Intelligent robots and systems, pp 2246–2251
20. Calals B (2007) Anatomy of movement, Revised edn. Eastland Press, Vista
21. Nordin M (2001) Basic biomechanics of the musculoskeletal system. Lippincott Williams & Wilkins, Philadelphia ISBN-13: 978-0683302479
22. Valero-Cuevas FJ, Johanson ME, Towles JD(2003) Towards a realistic biomechanical model of the thumb: the choice of kinematic description may be more critical than the solution method or the variability/uncertainty of musculoskeletal parameters. J Biomech 36(7):1019–1030
23. Santos VJ, Valero-Cuevas FJ (2006) Reported anatomical variability naturally leads to multimodal distributions of Denavit–Hartenberg parameters for the human thumb. IEEE Trans Biomed Eng 53(2):155–163
24. Chalon M, Grebenstein M, Wimbock T, Hirzinger G (2010) The thumb: guidelines for a robotic design. In: International conference on intelligent robots and systems, pp 5886–5893
25. Wang H, Fan S,LiuH(2012)Ananthropomorphic design guideline for the thumb of the dexterous hand. In: International conference on mechatronics and automation, pp 777–782
26. Martin J, Grossard M (2014) Design of a fully modular and backdrivable dexterous hand. Int J Robot Res 33(5):783–798
27. Calli B, Walsman A, Singh A, Srinivasa S, Abbeel P, Dollar AM (2015) Benchmarking in manipulation research: using the Yale–CMU–Berkeley object andmodel set. IEEE AutomMag 22(3):36–52
28. Bae JHS, Park W, Kim D, Baeg MH, Oh SR (2012) A grasp strategy with the geometric centroid of a groped object shape derived from contact spots. In: International conference on robotics and automation (ICRA), Minnesota, pp 3798–3804
29. Cutkosky MR, Howe RD (1990) Human grasp choice and robotic grasp analysis, Chapter 1. In: Venkataraman ST, Iberall T (eds) Dextrous robot hands. Springer, Berlin, pp 5–31